nearest flux lines in a constant z cross section (6). Both $G_6(q_\perp)$ and $G_6(q_\perp, L)$ have peaks (delta function) at $q_\perp = 0$. These peaks are effectively removed when taking the ratio of these two quantities to obtain the transfer function $R_H(q_\perp, L)$; however, we have been unable to determine reliably the small-q behavior of $G_6(q_\perp)$ alone (that is, to extract $\sqrt{c_{44}c_{66}}$ as was done in the case of 2D density correlations for $\sqrt{c_{11}c_{44}}$ because of this peak.

17. E. Frey, D. R. Nelson, D. S. Fisher, *Phys. Rev. B* **49**, 9723 (1994).
18. R. K. Pathria, *Statistical Mechanics* (Pergamon, New York, 1993).
19. D. R. Nelson, *Phys. Rev. Lett.* **60**, 1973 (1988); M. P. A. Fisher and D. H. Lee, *Phys. Rev. B* **39**, 2756 (1989).

20. We thank D. R. Nelson and M. C. Marchetti for helpful discussions. C.M.L. acknowledges support by the National Science Foundation (grant DMR 9306684) and the Materials Research Science and Engineering Center Program of the National Science Foundation (grant DMR 9400396).

10 May 1995; accepted 18 August 1995

A Class of Cobalt Oxide Magnetoresistance Materials Discovered with Combinatorial Synthesis

Gabriel Briceño, Hauyee Chang, Xiaodong Sun,
Peter G. Schultz,* X.-D. Xiang*

The recent development of methods for generating libraries of solid-state compounds has made it possible to apply combinatorial approaches to the discovery of materials. A library of 128 members containing different compositions and stoichiometries of $Ln_xM_yCoO_\delta$, where Ln = Y or La and M = Pb, Ca, Sr, or Ba, was synthesized by a combination of thin-film deposition and physical masking techniques. Large magnetoresistance has been found in $La_x(Ba,Sr,Ca)_y$-CoO_δ samples, whereas Y-based samples exhibit much smaller magnetoresistive effects. The magnetoresistance of the Co-containing compounds increases as the size of the alkaline earth ion increases, in sharp contrast to Mn-containing compounds, in which the magnetoresistance effect increases as the size of the alkaline earth ion decreases.

The discovery of the magnetoresistive effect (*1*) in Mn-based perovskite oxides $(La,R)_{1-x}A_xMnO_{3-\delta}$, where R is a rare earth element and A = Ca, Sr, or Ba, has attracted considerable attention because of the potential application of these materials in magnetic storage technology. Colossal magnetoresistance (CMR), with MR ratios $\Delta R/R(0) = [R(H = 0) - R(H)]/R(H = 0)$ as large as 99.0, 99.9, and 99.99%, have been reported for polycrystalline samples of $La_{0.60}Y_{0.07}Ca_{0.33}MnO_x$ and epitaxial thin films of $La_{0.67}Ca_{0.33}MnO_3$ and $Nd_{0.7}Sr_{0.3}MnO_{3-\delta}$, respectively (*2–4*). A large number of theoretical and experimental efforts have been undertaken to understand this unexpected phenomenon and to improve the room-temperature sensitivity, $[\Delta R/R(0)]/\Delta H$, at $H = 0$ of these materials, an important factor for technical applications. The question arises whether these effects are unique to Mn-based perovskite oxides or can be found as an intrinsic property of other materials.

We have applied a combinatorial approach (*5*) to the search for more CMR materials. Our initial search for CMR compounds was around simple perovskite ABO_3 and related A_2BO_4 or $A_{n+1}B_nO_{3n+1}$ higher order structures, where A = (La, Y, or rare earth)$^{+3}$ partially substituted with (Ca, Sr, Ba, Pb, or Cd)$^{+2}$ and B = (Mn, V, Co, Ni, Cr, or Fe). In this report, we describe a specific example of the generation and screening of one such library that resulted in the discovery of a family of Co-containing CMR materials. An analysis of the effects of spin configuration and electronic structure on the MR properties of the Co- and Mn-based compounds should help to elucidate the underlying mechanism of the CMR effect. Moreover, the discovery of diverse classes of the CMR materials may help efforts to optimize these materials for eventual device applications.

A 128-member library was generated by combining sequential radio-frequency sputtering deposition of thin films with a series of physical masking steps designed to produce Y-, La-, Ba-, Sr-, Ca-, and Co-containing films (1 mm by 2 mm) with varying compositions and stoichiometries (Fig. 1). Polished (100) $LaAlO_3$ single crystals were used as substrates and La_2O_3, Y_2O_3, $BaCO_3$, $SrCO_3$, CaO, and Co were used as sputtering targets (*6*). Two identical libraries (L1 and L2) were generated simultaneously and then thermally treated under different annealing and sintering

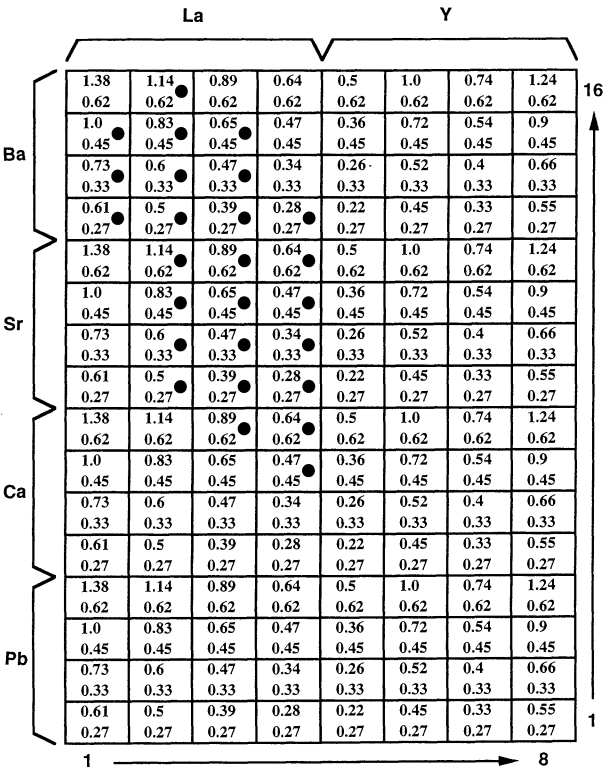

	La				Y			
Ba	1.38 0.62	1.14 0.62 ●	0.89 0.62	0.64 0.62	0.5 0.62	1.0 0.62	0.74 0.62	1.24 0.62
	1.0 0.45 ●	0.83 0.45 ●	0.65 0.45 ●	0.47 0.45	0.36 0.45	0.72 0.45	0.54 0.45	0.9 0.45
	0.73 0.33 ●	0.6 0.33 ●	0.47 0.33 ●	0.34 0.33	0.26 0.33	0.52 0.33	0.4 0.33	0.66 0.33
	0.61 0.27 ●	0.5 0.27 ●	0.39 0.27 ●	0.28 0.27 ●	0.22 0.27	0.45 0.27	0.33 0.27	0.55 0.27
Sr	1.38 0.62	1.14 0.62 ●	0.89 0.62 ●	0.64 0.62 ●	0.5 0.62	1.0 0.62	0.74 0.62	1.24 0.62
	1.0 0.45	0.83 0.45 ●	0.65 0.45 ●	0.47 0.45 ●	0.36 0.45	0.72 0.45	0.54 0.45	0.9 0.45
	0.73 0.33	0.6 0.33 ●	0.47 0.33 ●	0.34 0.33 ●	0.26 0.33	0.52 0.33	0.4 0.33	0.66 0.33
	0.61 0.27	0.5 0.27 ●	0.39 0.27 ●	0.28 0.27 ●	0.22 0.27	0.45 0.27	0.33 0.27	0.55 0.27
Ca	1.38 0.62	1.14 0.62	0.89 0.62 ●	0.64 0.62 ●	0.5 0.62	1.0 0.62	0.74 0.62	1.24 0.62
	1.0 0.45	0.83 0.45	0.65 0.45	0.47 0.45 ●	0.36 0.45	0.72 0.45	0.54 0.45	0.9 0.45
	0.73 0.33	0.6 0.33	0.47 0.33	0.34 0.33	0.26 0.33	0.52 0.33	0.4 0.33	0.66 0.33
	0.61 0.27	0.5 0.27	0.39 0.27	0.28 0.27	0.22 0.27	0.45 0.27	0.33 0.27	0.55 0.27
Pb	1.38 0.62	1.14 0.62	0.89 0.62	0.64 0.62	0.5 0.62	1.0 0.62	0.74 0.62	1.24 0.62
	1.0 0.45	0.83 0.45	0.65 0.45	0.47 0.45	0.36 0.45	0.72 0.45	0.54 0.45	0.9 0.45
	0.73 0.33	0.6 0.33	0.47 0.33	0.34 0.33	0.26 0.33	0.52 0.33	0.4 0.33	0.66 0.33
	0.61 0.27	0.5 0.27	0.39 0.27	0.28 0.27	0.22 0.27	0.45 0.27	0.33 0.27	0.55 0.27

Fig. 1. A map of compositions and stoichiometries ($Ln_xM_yCoO_{3-\delta}$, where Ln = La or Y and M = Ba, Sr, Ca, or Pb) of thin-film samples in libraries L1 and L2. Samples are labeled by index (row number, column number) in the text and figure legend. The first number in each box indicates x and the second y. Solid circles indicate the samples that show significant MR effects (>5%).

G. Briceño and X.-D. Xiang, Molecular Design Institute, Lawrence Berkeley Laboratory, Berkeley, CA 94720, USA.
H. Chang, X. Sun, P. G. Schultz, Molecular Design Institute, Lawrence Berkeley Laboratory, Howard Hughes Medical Institute, and Department of Chemistry, University of California, Berkeley, CA 94720, USA.

*To whom correspondence should be addressed.

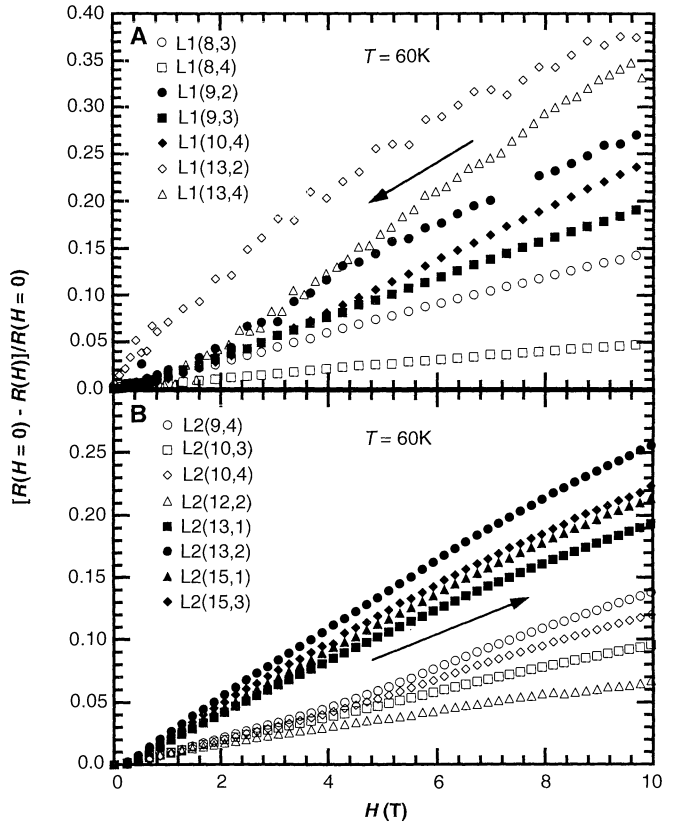

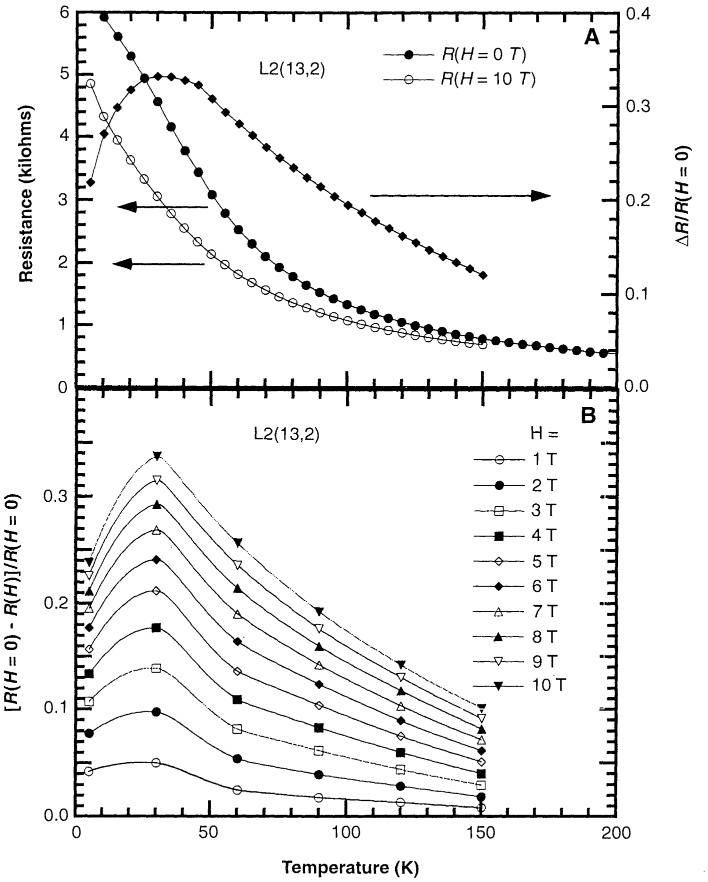

Fig. 2 (**left**). The MR ratios of representative samples in (**A**) L1 and (**B**) L2 as a function of magnetic field. **Fig. 3** (**right**). (**A**) Resistance of sample L2(13, 2) under 0 and 10 T and the MR ratio (H = 10 T) as a function of temperature; (**B**) MR ratios of the same sample for different magnetic fields as a function of temperature. The solid lines are guides to the eye.

procedures (up to 900°C) in O_2 or air (7). Figure 1 indicates the composition and stoichiometry of each sample. The resistivity of each sample as a function of magnetic field (perpendicular to the probing current) and temperature was measured by the four-probe contact method with a computer-controlled multichannel switching system. A liquid-helium cryogenic system with a superconducting 12-T magnet was used to perform variable-temperature and -field measurements.

A number of films in the library showed a significant (>5%) MR effect (Fig. 1, solid circles). Three compounds that exhibit a large giant-MR effect have been identified: $La_xM_yCoO_\delta$, where M = Ca, Sr, or Ba. The normalized MRs of representative samples as a function of magnetic field at fixed temperature (60 K) are shown in Fig. 2; the temperature dependence of the resistance and normalized MR of a representative sample, L2(13, 2), under different fields are shown in Fig. 3. In contrast to the behavior of Mn oxide MR materials (2, 3), the MR effect increases as the size of the alkaline earth ion increases (Fig. 2).

The MR effects of the samples in library L1 are larger than those of L2, presumably because of differences in oxidation resulting from slightly different thermal treatments. The largest MR ratio measured in this library was 72%, obtained for sample L1(15, 2) at $T = 7$ K and $H = 10$ T. This value is comparable to those measured for films generated in a similar fashion in a Mn-based library (8). As with the Mn-containing materials, optimization of composition, stoichiometry, substrate, and synthetic conditions may lead to increases in the MR ratio. The corresponding Y-(Ba,Sr,Ca)-Co compounds show much smaller (<5%) MR effects.

Three bulk samples with the stoichiometry $La_{0.67}(Ba,Sr,Ca)_{0.33}CoO_\delta$ were then synthesized (sintered at 1400°C in air) for further structural study. The x-ray diffraction patterns show that the crystal structure is basically cubic perovskite with lattice constant $a = 3.846$, 3.836, and 3.810 Å for the Ba, Sr, and Ca compounds, respectively. Minor splittings of the intensity peaks are attributed to rhombohedral distortion from the perfect cubic perovskite structure (9).

A bulk sample of stoichiometry $La_{0.58}Sr_{0.41}CoO_\delta$ was synthesized and its magnetization was measured with a superconducting quantum interference device (SQUID) magnetometer. The sample MR as a function of magnetic field and the sample magnetization under a 1-T magnetic field as a function of temperature were measured (Fig. 4). A gradual ferromagnetic transition starts at ~200 K and saturates below 50 K. The MR ratio of this bulk sample (60%) is

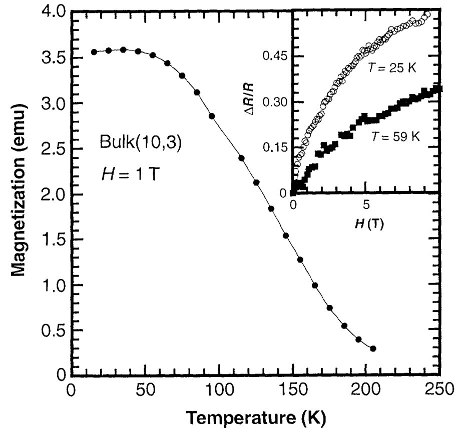

Fig. 4. Magnetization of the bulk sample $La_{0.58}Sr_{0.41}CoO_\delta$ under a 1-T field as a function of temperature. The solid line is a guide to the eye. (**Inset**) MR ratios of the sample at different temperatures as a function of magnetic field.

significantly higher than that of the corresponding thin-film sample in L1 (30%). The x-ray analysis of this sample confirmed the cubic perovskite structure with $a = 3.82$ Å.

It has been suggested (*3*) that the CMR effect in the Ca-doped $LaMnO_3$ system originates from "double exchange" electron-hopping processes between Mn^{3+} and Mn^{4+} neighboring sites through the O^{2-} anion between them (*10*). In these processes, the e_g itinerant electron conduction or hopping rate $t_{ij} = t_0\cos(\theta_{ij}/2)$, where θ_{ij} is the angle between local spin directions of electrons on neighboring sites i and j, and t_0 is the hopping rate in a perfect ferromagnetic state. The application of an external field may align the disordered local spins during a ferromagnetic transition and thereby increase electron conduction or even induce an insulator-metal transition through strong interaction between itinerant electron and local spins. In this model, the MR effect may be induced by an external field when the system is in transition toward the ferromagnetic state. In this aspect, our data are consistent with this model, that is, MR effects appear only below the Curie temperature ($T_c \sim 150$ to 200 K) and decrease below the saturation field ($\sim$30 to 40 K) (Fig. 3). However, the role of alkaline earth ion size in the MR effect remains unclear. In doped $LaMnO_3$ systems, it appears that smaller dopant size favors the MR effect (*5*), whereas in doped $LaCoO_3$ systems, the opposite effect is observed.

REFERENCES AND NOTES

1. See, for example, R. M. Kusters, J. Singleton, D. A. Keen, R. McGreevy, W. Hayes, *Physica B* **155**, 362 (1989); K. Chahara, T. Ohno, M. Kasai, Y. Kozono, *Appl. Phys. Lett.* **63**, 1990 (1993); H. L. Ju, C. Kwon, R. L. Greene, T. Venkatessan, *ibid.* **65**, 2108 (1994); R. von Helmolt, J. Wecker, K. Samwer, L. Haupt, K. Bärner, *J. Appl. Phys.* **76**, 6925 (1994).
2. S. Jin, H. M. O'Bryan, T. H. Tiefel, M. McCormack, W. W. Rhodes, *Appl. Phys. Lett.* **66**, 382 (1995).
3. S. Jin *et al.*, *Science* **264**, 413 (1994).
4. G. C. Xiong *et al.*, *Appl. Phys. Lett.* **66**, 1427 (1995).
5. X.-D. Xiang *et al.*, *Science* **268**, 1738 (1995).
6. Sputtering was carried out at 5 to 15 mtorr, with Ar as the sputtering gas; deposition rates were 0.1 to 1 Å s^{-1}. Film thickness was monitored with a crystal microbalance and calibrated independently with a profilometer. The uniformity of the deposited films varied less than 5% over an area ~2.5 cm in diameter.
7. Library L1 was treated as follows: heated from room temperature (RT) to 200°C, heated to 300°C over 12 hours, and cooled to RT; it was then heated to 650°C over 1 hour, heated to 850°C over 3 hours, heated to 900°C over 3 hours, and cooled to RT over 2 hours. Library L2 was treated as follows: heated from RT to 200°C, heated to 350°C over 15 hours, and cooled to RT; it was then heated to 650°C over 2 hours, heated to 740°C over 13 hours, heated to 850°C over 1 hour, heated to 900°C over 0.5 hour, cooled to 650°C over 2 hours, and cooled to RT.
8. G. Briceño, X. Sun, H. Chang, X.-D. Xiang, P. G. Schultz, unpublished material.
9. F. Askham, I. Fankuchen, R. Ward, *J. Am. Chem. Soc.* **72**, 3799 (1950).
10. C. Zener, *Phys. Rev.* **82**, 403 (1951); P. W. Anderson and H. Hasegawa, *ibid.* **100**, 675 (1955); P.-G. de Gennes, *ibid.* **118**, 141 (1960).
11. We are grateful for financial support for this work from the Laboratory Directed Research and Development Program of Lawrence Berkeley Laboratory under U.S. Department of Energy contract DE-AC03-76SF00098 and the Office of Naval Research (grant N00014-95-F-0099). G.B. acknowledges support from a University of California President's Postdoctoral Fellowship. We thank J. Torrance for helpful advice and E. Granlund and J. Wu for technical support.

25 May 1995; accepted 22 August 1995

Molluscan Diversity in the Late Neogene of Florida: Evidence for a Two-Staged Mass Extinction

Edward J. Petuch

Analyses of recent data show that Floridian molluscan diversity declined markedly during the Pliocene-Pleistocene mass extinction. This decline in diversity was seen at all trophic levels, indicating a complete collapse of the ecosystem. These findings contradict the notion that there was a species diversity stasis throughout the Pliocene-Pleistocene and that the diversity of Pliocene Florida was equivalent to that of Recent Florida. The mass extinction was a two-staged, sequential event. A similar two-staged mass extinction occurred in the Miocene, indicating that two ecological catastrophes in quick geological succession may have produced this mass extinction as well.

Studies of tropical western Atlantic Pliocene (Plio)-Pleistocene molluscan mass extinctions (*1–8*) have resulted in two conflicting conclusions. The main data source used to arrive at these antitheses was the rich upper Neogene molluscan fossil beds of southern Florida (deposited within the Floridian component of the Plio-Pleistocene Caloosahatchian Molluscan Province) (*2, 6, 9*). One conclusion (*4*) was that diversity (at both the generic and specific levels) decreased dramatically in Florida during late Pliocene–early Pleistocene time, producing an impoverished middle and late Pleistocene fauna and a reconstituted but less diverse Recent Floridian fauna. The other conclusion (*8*) was that although Plio-Pleistocene rates of extinction were high in Florida, the overall diversity (species level) has remained relatively constant from the Pliocene to the Recent. This was explained by a high rate of recruitment (origination), produced by invasion and speciation, that balanced the net loss due to extinction. Both notions, however, were hampered by incomplete museum collections and by variable reporting in the literature.

Data sources and compendia have recently become available that offer a more complete database of molluscan diversity (*10, 11*). When put into a new stratigraphic and geochronological scheme (*12, 13*), the data on macrogastropod diversity reveal patterns of extinction and faunal impoverishment. In an attempt to illustrate such patterns, I selected eight dominant macrogastropod families for analysis, with each representing a major trophic level within its respective molluscan community. Included are algal film grazers (Potamididae), sea grass and epibiont feeders (Cypraeidae), suspension and detritus feeders (Turritellidae), large general carnivores (Busyconidae), small general carnivores (Buccinidae), molluscivores (Muricidae), vermivores (Conidae), and specialized suctorial feeders (Cancellariidae). If a mass extinction truly occurred, with a corresponding drop in species diversity, it would be safe to assume that many, if not all, trophic levels within an ecosystem would suffer.

As can be seen in Table 1 and Fig. 1, all eight families reached a peak of species diversity during the middle Pinecrest Beds (PB2, units 5, 6, 7) at approximately 3 million years ago (Ma) (*14*). Species diversity declined at the end of Pinecrest Beds time, rose again during Caloosahatchee time, at approximately 1.5 to 2 Ma, and then dropped precipitously during the late Pleistocene (Bermont to Fort Thompson interval). With the exception of the Conidae, with five additional species, and the Potamididae, with an equivalent number of species, all other families show a much lower species diversity in Recent Florida. If all three Pinecrest Beds faunas are considered in unison, as in (*8*), then the total number of Pinecrest Beds species is much larger for all eight families. In the case of some families, such as the Busyconidae, the difference between the late Pliocene Pinecrest Beds and the Recent fauna is over eightfold. Other families, such as the Cypraeidae, Turritellidae, and Cancellariidae, all exhibit differences ranging from factors of 4 to over 5. The same pattern is seen at the generic level, as shown in Table 2. With the exception of the Cypraeidae (because of late Pleistocene inva-

---

Division of Geological Oceanography, Department of Geology, Florida Atlantic University, Boca Raton, FL 33431, USA.